Hindawi
Geofluids
Volume 2020, Article ID 2648692, 12 pages
https://doi.org/10.1155/2020/2648692

Research Article

Dynamic Evaluation Method of Caprock Microscopic Sealing in CO_2 Sequestration Project

Xu Han,[1,2] Fuping Feng,[1,2] and Ziyuan Cong[1,2]

[1]*Department of Petroleum Engineering, Northeast Petroleum University, Daqing 163318, China*
[2]*Key Laboratory of Enhanced Oil Recovery (Northeast Petroleum University), Ministry of Education, China*

Correspondence should be addressed to Fuping Feng; fengfuping2005@nepu.edu.cn

Received 23 August 2019; Accepted 26 November 2019; Published 3 March 2020

Academic Editor: Francesco Frondini

The existing statistical evaluation methods of caprock sealing ability in CO_2 sequestration engineering only take into account the sealing ability of caprocks before sequestration but cannot reflect the retained sealing ability of caprock after hydrochemical reactions. A microscopic sealing evaluation method of caprock was established based on the microscopic mechanism of chemical reaction and the breakthrough pressure of caprock which, changes with the time of CO_2 sequestration, was taken as the dynamic evaluation index. The results show that the change of microstructure parameters such as the average pore radius after dissolution is the essential reason that affects the variation of the caprock microscopic sealing property. Dissolution or precipitation of different caprock minerals during the chemical reaction process is the key factor that determines the decrease or increase of caprock microscopic sealing property. The evaluation method can reflect the change of microscopic sealing property of the caprocks in different areas as the sealing time goes and provides an efficient and practical quantitative evaluation method for the initial formation site selection and safety sealing in the later stage.

1. Introduction

CCUS (carbon capture, utilization, and storage) technology is widely used in major oilfields as a significant method of energy conservation and pollution emission reduction combined with the displacement of reservoir oil. From the interest of oil and gas field development, oil recovery has been increased by more than 10% through the CO_2 flooding technology in China [1]. However, from the interest of environmental protection, although CO_2 underground storage can reduce the greenhouse gas content of the air, whether it can be safely stored in the formation has become a new problem facing humanity.

In recent years, scholars at home and abroad have carried out a large number of related studies on geochemistry problems related to the site selection and application of CO_2 flooding and burial projects. Figure 1 shows the three ways that trapped CO_2 mainly leaks and escapes through in the reservoir: permeation and escape from caprock, diffusion and escape from caprock, and escape from caprock fractures or abandoned wells [2–4]. The change of gas saturation generally goes through two stages: first, it increases from the bottom of the barrier layer to the top successively with time, until it breaks through the caprock, leakage occurs, and then decreases gradually. The changes of rock physical properties are consistent with the spatial distribution characteristics of CO_2 gas saturation [5].

CO_2 sequestration capacity is mainly controlled by permeability, connectivity, pore volume, injection well type, and other factors of caprock [6]. Based on the current geological model, these are the most influential parameters to determine the potential for successful CO_2 geological storage of CO_2. However, CO_2 leakage also has a substantial impact on the geochemical evolution of caprock [7]. CO_2-water-rock chemical reaction process is often accompanied by mineral dissolution and precipitation, seriously threatening the safety of CO_2 geological sequestration. When CO_2 fluids driven by buoyancy migrate upward through the microcracks of rocks and form channels, chemical reactions cause a large number of mineral dissolution and alter the caprock microstructure.

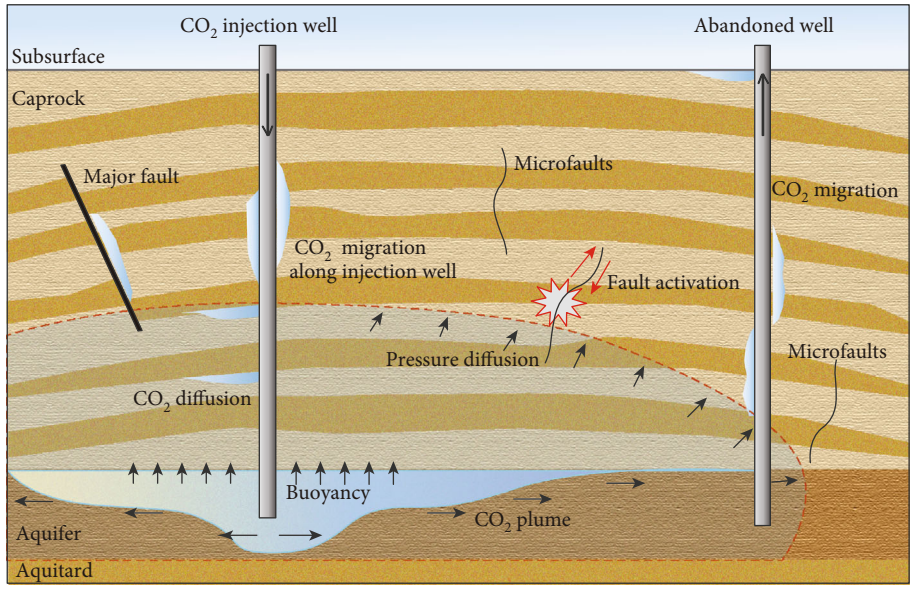

Figure 1: CO_2 migration of sequestration and leakage process.

On the contrary, precipitation of secondary minerals can further improve the caprock sealing ability. Li et al. [8] simulated the diffusion and migration processes of CO_2 in the formation under long-term storage and found that CO_2 invaded the caprock from 10 to 46 meters with different formation conditions and initial minerals. Kong et al. [9] simulated and calculated the transport of CO_2 in the formation and the change of gas saturation at different positions. CO_2 was injected at 24 MPa continuous constant inject pressure for 10000 years. The gaseous CO_2 entered the caprock after ten years in large quantities and reached 69 meters away from the injection point, and the vertical migration dimension reached 125 m after 120 years.

Therefore, the evaluation of caprock sealing safety should not only include the blocking effect on the CO_2 vertical transport but also include the studies on the damage caused by the acidic solution of CO_2 and the caprock sealing property changes after long-term sequestration.

The caprock sealing mechanism mainly includes microsealing and macrosealing. In addition to strong microsealing ability, the caprock also needs to have a specific sufficient thickness and macrodistribution area to seal CO_2 in the formation system effectively [10–14]. At the present stage, most evaluation methods of caprock sealing property are multifactor evaluation methods based on statistics [15], such as the fuzzy evaluation method or weighted analysis method. The main disadvantage of these methods, which is suitable for solving problems with many uncertain factors, is that the subjective factors account for a relatively high proportion in the evaluation and the accuracy is relatively low. However, these methods are no longer suitable for the caprock microsealing mechanism. Other plans start from the breakthrough pressure and integrate the sedimentary environment, logging data, pore structure parameters, laboratory test parameters, and different kinds of rock data; the classification evaluation standards of caprock sealing capacity were established, respectively, and provided a theoretical basis for the gradual quantitative evaluation of caprock safety [16–21].

In the above evaluation methods of the caprock sealing capacity, the evaluation criteria obtained by laboratory experiments are not in line with the actual strata numerically. This is due to the significant difference between the actual formation states and the laboratory conditions, which is mainly reflected in the following two aspects: first, the rock skeleton is stressed by the overlying strata, and most of the pores are in a compressed state; second, the temperature environment of the formation will also change with the temperature system of each layer, and the temperature at different depths varies greatly; liquid viscosity and gas phase will also change with the temperature. The parameters of the caprock are obviously different from those at standard temperature and pressure. Therefore, these methods are only applicable to stable gas which does not react with formation. Without taking into account the influence of chemical reaction on the caprock microstructure after CO_2 invasion, these methods have difficulty evaluating the microscopic sealing property of caprock accurately under long-term sealing and reacting conditions.

In this paper, the change of breakthrough pressure with time is taken as the dynamic evaluation index, and the microsealing evaluation method is established based on the microscopic mechanism of caprock chemical reactions. The caprock microscopic sealing property of an oilfield is analyzed and evaluated by using the actual data of CO_2 flooding and sequestration project with this method.

2. Microcosmic Sealing Evaluation Method of CO_2 Geological Sequestration

2.1. Mechanism of Caprock Microscopic Sealing. The mechanism of caprock microscopic sealing includes capillary

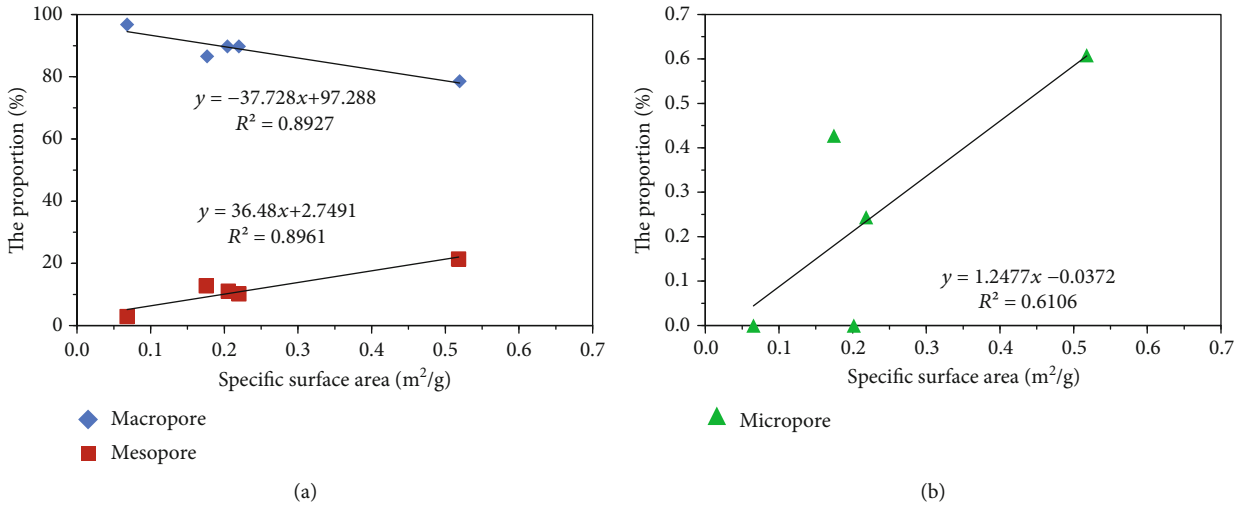

Figure 2: Correlations between proportions of macropores, mesopores, micropores, and specific surface area.

sealing, hydrocarbon concentration sealing, and overpressure sealing. For CO_2 sequestration formation, when the barrier layer is not capable of generating hydrocarbon and there are no overpressure sites, the mechanism of caprock microscopic sealing is mainly embodied as capillary seals. It depends on the difference in capillary pressure between the reservoir and the caprock. The higher the difference is, the stronger the physical sealing ability will be [22]. At present, the breakthrough pressure, permeability, porosity, density, specific surface area, and micropore structure of rocks are widely used to evaluate the microsealing ability of caprock. The breakthrough pressure is the most direct and fundamental microscopic sealing parameter among them. The functional relationship between breakthrough pressure and porosity, permeability, density, median pore radius, and specific surface area in different oil-bearing basins in China shows that [23–25] the breakthrough pressure has an approximately linear relationship with other micropore structure parameters. These physical parameters can be replaced by the breakthrough pressure (BP) of the caprocks in the evaluation of microscopic sealing (Figures 2–4).

With the decrease of porosity, permeability, and the median radius of pores and the increase of density and specific surface area, the breakthrough pressure of rocks will increase. On the contrary, rock breakthrough pressure will decrease.

Therefore, these physical parameters can be replaced by the breakthrough pressure of the caprocks in the evaluation of microscopic sealing. According to Washburn theory, the relationship between capillary pressure and the median pore radius can be expressed as follows [25]:

$$P_c = \frac{2\sigma \cos\theta}{r}, \quad (1)$$

where P_c is the breakthrough pressure, MPa; σ is the fluid interfacial tension, Pa; θ is the fluid wetting angle; r is the median pore radius, m.

It can be seen from the above equation that for the same fluid, the size of the median pore radius is the decisive factor for the breakthrough pressure of the caprock. When considering the effect of CO_2 fluid intrusion on the internal microstructure of the caprock, the pore radius will gradually increase with the dissolution of primary minerals. The pores and microcracks will be formed in the caprock microstructure, thus weakening its microscopic sealing ability. On the contrary, if precipitation reaction occurs, the microscopic sealing ability will be enhanced. Therefore, the evolution of the caprock microscopic sealing property can be attributed to the change of rock microstructure caused by chemical reactions.

2.2. Evaluation Method of Caprock Microscopic Sealing. The caprock microscopic sealing process of CO_2 can be equivalent to the process of rock microstructure change under acidic conditions. The mineral composition in caprocks can be roughly divided into carbonate minerals, feldspar minerals, clay minerals, and quartz. Each mineral has complex chemical reactions with CO_2 based on its specific dissolution or formation conditions. Therefore, the initial mineral composition and chemical reaction mechanism are the key factors to evaluate the caprock microscopic sealing ability. The dynamic variation rule of rock porosity and permeability can be obtained by calculating the process of mass conservation of each mineral during CO_2 sequestration. The relationship between rock microstructure and breakthrough pressure is used to calculate the change of caprock breakthrough pressure under the influence of chemical reactions, and the sealing performance of the caprock is classified according to different value ranges of the gas column that the rock can seal.

During the CO_2-water-caprock reaction, the volume fraction of each mineral changes, and then the porosity changes at each time step of the calculation. The mass conservation principle is used to calculate the mass and volume changes of every mineral phase and update the volume fraction.

$$\phi_{j,i,t+\Delta t} = \phi_{j,i,t} + V_j \times R_{j,i,t+\Delta t} \times \Delta t, \quad (2)$$

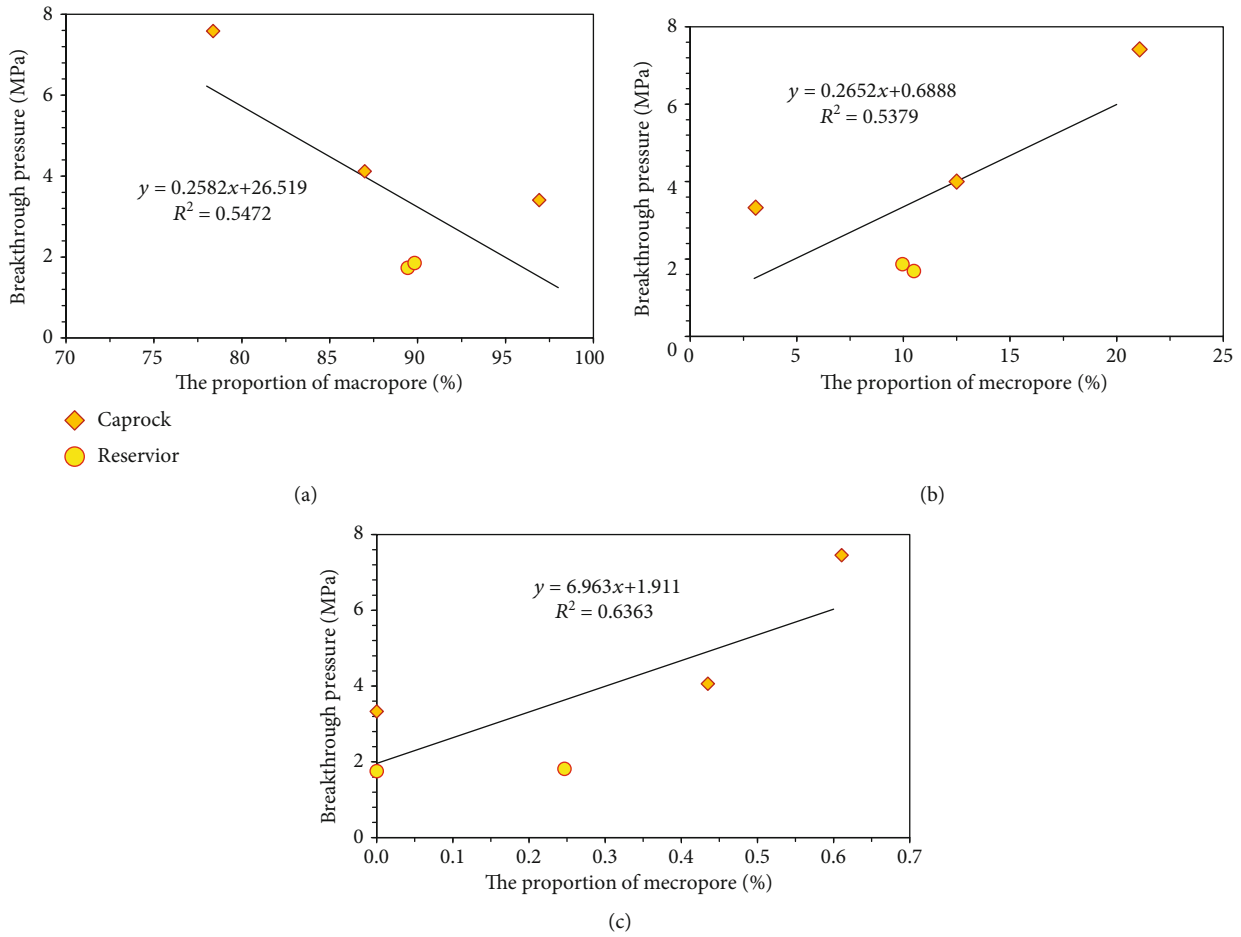

Figure 3: Relationships between proportions of macropores (a), mesopores (b), micropores (c), and BP.

where $\phi_{j,i,t}$ is the volume fraction of mineral j in region i at t time, V_j is the molar volume of mineral j, and $R_{j,i,t+\Delta t}$ is the reaction velocity of mineral j in region i at t time.

According to the law of chemical kinetics, the rate of mineral dissolution or precipitation reaction follows the formula [26]:

$$\mathrm{R}_\beta = \widehat{\mathrm{A}}_\beta k_\beta \left(1 - \frac{\mathrm{Q}}{K_{\mathrm{eq},\beta}}\right), \beta = 1, \cdots, \zeta_{\mathrm{mn}}, \tag{3}$$

where ζ_{mn} is the amount of reactions, R_β is the velocity of reactions, mol/L·s^{-1}, A is the reactive surface area of mineral, m^2, k_β is the reaction rate constant, and K_{eq} is the equilibrium constant of reaction. Kharaka and Yousif [27] and Businger and Delany [28] listed the numerical value of K_{eq} as a function of temperature. $Q/K_{\mathrm{eq},\beta}$ is the saturation index of the reaction, if $Q/K_{\mathrm{eq},\beta} - 1$, mineral dissolution occurs. Otherwise mineral precipitation occurs; Q is the activity product:

$$\mathrm{Q}_\beta = \prod_{k=1}^{n_{\mathrm{aq}}} a_k^{\nu_{k\beta}}, \tag{4}$$

where n_{aq} is the number of ions in the solution, a_k is the activity of the reactive component, $\nu_{k\beta}$ is the stoichiometric coefficient of equilibrium reaction, the stoichiometric coefficient of reactants is negative, and the product is positive.

The formation or consumption rates of different minerals can be calculated by multiplying A by the respective metrology coefficients:

$$R_{k\beta} = \nu_{k\beta} \times R_\beta. \tag{5}$$

k_β is the rate constant of chemical the reaction:

$$k_\beta = k_{0\beta} \exp\left[\frac{-E_{\alpha\beta}}{R(1/T - 1/T_0)}\right], \tag{6}$$

where $E_{\alpha\beta}$ is the activation energy of reaction β, R is the molar gas constant, and $k_{0\beta}$ is the reaction rate constant of reaction β at T_0 (298.15 K usually); it can be calculated by the Arrhenius equation:

$$k_{0\beta} = A(T)e^{-(E_a/RT)}. \tag{7}$$

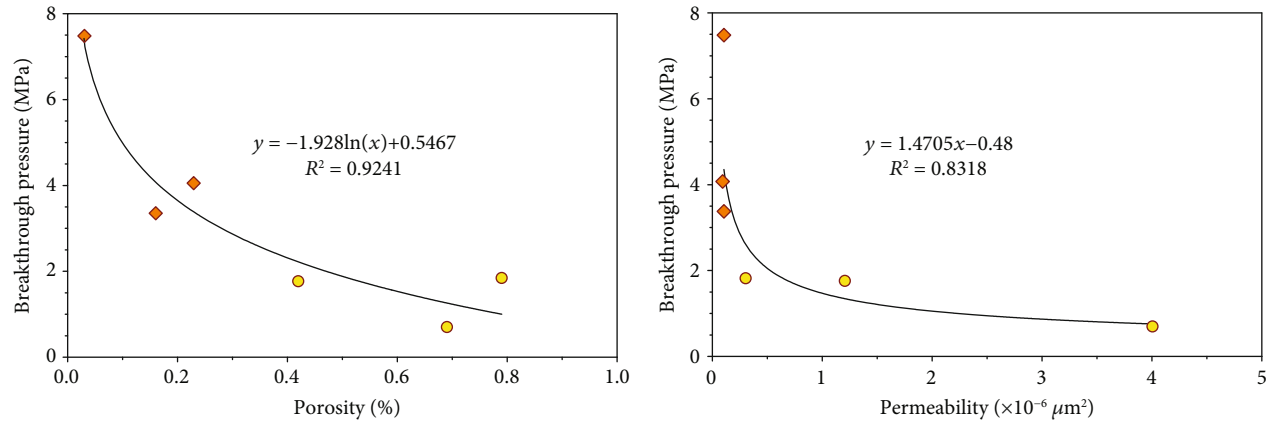

Figure 4: Behavior of the BP with effective porosity (a) and permeability (b).

The change in the volume of every single mineral can be obtained by multiplying reaction rate by molar volume; the changes in caprock porosity caused by chemical reactions can be replaced by the changes in the volume of the minerals involved in the chemical reactions. The rock porosity can be calculated by the following equation:

$$\phi = 1 - \sum_{m=1}^{N_m} \phi_m, \tag{8}$$

where N_m is the number of mineral species in the rock and ϕ_m is the volume fraction of every mineral.

Matrix permeability changes are calculated from changes in porosity using ratios of permeabilities calculated from the Carman-Kozeny relation and ignoring changes in grain size, tortuosity, and specific surface area [29]:

$$k = k_0 \frac{(1-\phi_0)^2}{(1-\phi)^2} \left(\frac{\phi}{\phi_0}\right)^3, \tag{9}$$

whereϕ_0, $\phi$are, respectively, the rock porosity in the grid before and after the reactions and k_0, k are, respectively, the rock permeability in the grid before and after reactions, m^2.

The Kozeny model regards porous media as a bundle of capillary tubes model composed of matrix and pores with uniform radius distribution. According to the Poiseuille formula, the flow rate of the entire section is [30]

$$Q = nA \cdot q = \frac{\pi n A \Delta p}{8\tau\mu\Delta l} \cdot (r_1 - r_0)^4 = \frac{\pi r^4 n A \Delta p}{8\tau\mu\Delta l}, \tag{10}$$

where q is the average single-hole flow rate of the capillary bundle mode, m^3/s; r is the pore radius difference between before (r_0) and after (r_1) the reaction, μm; n is the capillary number of flow area; A is the section area of a single capillary, m^2; Δp is the pressure difference at both ends of the pore, MPa; μ is the viscosity of the fluid, mPa·s; ΔL is the pore length, m.

According to Darcy's law, the permeability of rock is

$$Q = \frac{knA\Delta p}{\mu\Delta l}. \tag{11}$$

Combined with the Darcy law equation, the relation between the pore median radius and the permeability can be obtained by the following equation [31]:

$$k = \frac{\pi r^4}{8\tau}, \tag{12}$$

where τ is tortuosity; it represents the degree of tortuosity of the channel.

By combining the above equation, the relationship between rock breakthrough pressure and dynamic changes in porosity and permeability caused by dissolution can be calculated:

$$P_c{}' = \frac{2\sigma\cos\theta}{\sqrt[4]{\left((8\tau k_0(1-\phi_0)^2)/\pi(1-\phi)^2\right)\cdot(\phi/\phi_0)^3}}. \tag{13}$$

The breakthrough pressure of formation rocks after CO_2 injection can be converted to equivalent air column sealing height. The air column sealing height is taken as the evaluation index, and the specified grade of the caprock [32] can be used to evaluate the caprock microscopic sealing property. When the height of the CO_2 column accumulates at the bottom of the caprock and exceeds the maximum sealing height of the layer, the caprock capillary pressure will be broken; CO_2 will displace the fluid in the upper formation until it escapes through the caprock, leading to the failure of the microscopic sealing ability. Smith's (1966) formula can be used to obtain the height of the sealing gas column at the caprock-reservoir interface under breakthrough pressure:

$$T_h = \frac{P_c{}'}{\left(\rho_w - \rho_{co_2}\right)g}, \tag{14}$$

where ρ_w is the density of the formation water, kg/m^3; ρ_{co_2} is the density of supercritical CO_2 fluid; g is the acceleration of gravity, 9.8 N/kg; T_h is the column height of gas sealing under P_c, m.

When the above method is applied to evaluate the microscopic sealing property of CO_2 storage formation, a specific analysis should be carried out in combination with different initial mineral compositions and geological conditions of the formation. For example, some caprocks have a high content of feldspar minerals, the dissolution of primary minerals is higher than that of secondary minerals, and the caprock microscopic sealing ability becomes worse. However, if the clay mineral content of some caprock is high, the precipitation reaction will be dominant and the pore volume will expand after fluid saturation, which is helpful in improving the sealing ability of caprock [33].

3. Application and Results

3.1. Simulation Methods. X oilfield is one of the most essential oil-bearing basins in China, containing precious oil and gas resources. With the development of the CO_2 flooding project, the rate of oil and gas recovery increases year by year. At the same time, considering that CO_2 geological storage is an effective method to slow down the national greenhouse effect; if oil and gas are exhausted, the original oil and gas reservoirs will provide enough storage space for CO_2. According to geological data, CO_2 injection layer in X oilfield belongs to low porosity and ultra-low permeability medium and deep clastic rock reservoir. The main caprock and its sealing performance play an important role in controlling CO_2 sequestration. In this section, the mudstone caprock of the second layer of this oilfield is selected as an example, and the above evaluation method is used to dynamically evaluate the impact of CO_2 storage on its microscopic sealing property.

3.1.1. Model Description. In this paper, a two-dimensional radial model with injection well as the left boundary, vertical formation thickness of 273 m, and horizontal distance of 1000 m is established by using the software TOUGHREACT, a numerical simulation software for reactive solute transport. The dynamic process of chemical reaction in the reservoir and the barrier after CO_2 storage is simulated. The change of rock breakthrough pressure is simulated by calculating the changes of microstructure parameters such as porosity, permeability, and pore throat radius caused by a chemical reaction to describe the dynamic change process of the microsealing ability of the caprock with the storage time.

The physicochemical reaction process between CO_2, brine, and minerals after CO_2 injection into the formation mainly includes the following three steps:

(1) Solute migration process: when CO_2 is injected into the reservoir, convection and diffusion of the ions in the acid solution will occur. Convection is the migration process of ions in solution with pore water flow. In this simulation, buoyancy is the only force driving fluid natural convection except for solute transport. The change in concentration gradient causes a diffusion phenomenon. The ions will diffuse from high concentration zone to low concentration zone and finally, tend to equilibrium

(2) Chemical reaction process: when the ions migrate to the surface of minerals, they will react with minerals, dissolve to form free ions, or precipitate to form secondary minerals. The transport reaction process of reactive ions in a chemical solution obeys the law of mass conservation, that is, the decrease of solute concentration through any unit is equal to the sum of convection, diffusion, and reaction [34].

$$\frac{\partial(\phi C_j)}{\partial t} = \nabla\left(D\phi\nabla C_j - \phi v C_j\right) + \sum_{j=1}^{M_j}\phi R_j = 0, \quad (15)$$

where ϕ is the porosity of rock; C_j is the concentration of material j, mol · L^{-1}; D is the diffusion coefficient, m^2 · s^{-1}; R_j is the reaction rate of material j, mol · L^{-1} · s^{-1}; M_j is the amount of materials.

(3) Physical properties of rock alteration process: under the reaction process of solution migration, minerals in rocks will have dissolution reaction and precipitate reaction. Dissolution is mineral dissolution and the generated ionic substances will migrate out of the pores, resulting in porosity increase. Precipitation will lead to a large number of secondary mineral particles attached to the surface of minerals or block small pores with solute migration. The final result leads to the change of rock micropore structure, which can seriously affect the ability of rock to maintain breakthrough pressure

3.1.2. Parameters Used in the Simulation. The mudstone data in the X area shows that the depth of the caprock is about 2400-2590 m, and the depth of the reservoir is about 2590~2653 m. The rocks are assumed to be isotropic homogeneous materials and there is no abnormal high temperature or high pressure. The remaining parameters are shown in Table 1.

Before the CO_2-water-rock reaction, the initial mineral content in the model and the initial solution ion concentration at the boundary are shown in Table 2. In order to facilitate the comparison of the migration rule and reaction process of CO_2 and the brine in the reservoir and caprock, the same initial ion concentration was set in both reservoir and barrier layer during this simulation, and each mineral is evenly distributed in the reservoir and the barrier according to its mass fraction.

3.1.3. Initial and Boundary Conditions. The mesh pressure of the caprock was set as the initial hydrostatic pressure, and the initial saturation of CO_2 saturation is set as 0. Because the whole reaction process is carried out in a closed

Table 1: Parameters of reservoir and caprock.

Stratum	Upper caprock	Reservoir	Caprock at bottom
Depth (m)	2400~2590	2590~2653	2653~2673
Accumulated thickness (m)	190	63	20
Density (kg·m^3)	2600	2400	2600
Porosity	0.072	0.15	0.02
Permeability (m^2)	6.9×10^{-20}	1.3×10^{-17}	8×10^{-21}
The ratio of horizontal to vertical permeability	10	10	10
Average temperature (°C)	90	97.3	100
Median pore radius (μm)	0.036	0.1	0.015

Table 2: Initial mineral and hydrochemical composition of X oilfield formation.

Initial mineral content of reservoir (%)								
Quartz	Feldspar		Carbonatite			Clay		
	K-feldspar	Plagioclase	Dolomite	Calcite	Dawsonite	Kaolinite	Illite	Montmorillonite
30.18	7.65	37.35	9.46	7.16	4.73	1.73	0.57	1.17
Initial mineral content of caprock (%)								
Quartz	Feldspar		Carbonatite			Clay		
	K- feldspar	Plagioclase	Dolomite	Calcite	Dawsonite	Kaolinite	Illite	Montmorillonite
19.67	4.85	28.93	9.55	12.37	3.5	4.64	8.16	8.33
Initial composition of formation water (mol·kg^{-1} H_2O)								
H^+	1.64×10^{-8}	Al^{3+}	5.57×10^{-7}	Fe^{2+}	6.12×10^{-3}	K^+		0.5100
SiO_2	8.64×10^{-4}	OH^-	5.66×10^{-5}	Ca^{2+}	0.161	Mg^{2+}		0.0344

Reaction equation [35–37]	log K_{eq}	Reaction rate constant k
Quartz $\Longleftrightarrow SiO_2(aq)$	-2.762	-15.63-
Kaolinite + $6H^+ \Longrightarrow H_2O + 2Al^{3+} + 2SiO_2(aq)$	4.3024	11.52
Calcite + $H_2O + CO_2 \Longleftrightarrow Ca^{2+} + 2HCO_3^-$	1.235	-10.03
Dolomite + $2H^+ \Longrightarrow Ca^{2+} + Mg^{2+} + 2HCO_3^-$	2.2247	-9.744
K-feldspar + $2H^+ + 9H_2O \Longrightarrow 2K^+ + 4H4SiO4$ + kaolinite	-0.481	-12.13

environment, only considering the inflow of CO_2 and no mass exchange with the outside, the solution concentration will gradually change with the reaction time, and this changing law is subject to the chemical rate equation of water-rock reaction, so the initial conditions ($t = 0$) are

$$Sg_{CO_2}(t)|_{\partial t} = 0, \quad C_i(t)|_{\partial\Omega} = C_0 - R_{k\beta}. \tag{16}$$

There are 24 grids in the horizontal direction and 17 grids in the vertical direction, with 408 grids in total. Small grids are used in the reservoir and the upper caprock that is near the injection well, and large grids are used in other areas. The boundary conditions and the grid division of the numerical simulation model are shown in Figure 5. The left side is the flow inlet, and no flow boundary will be set at the right, top and bottom at any time. The injection volume of carbon dioxide is set as 30 t/d.

3.2. Results and Discussion

3.2.1. Gas Saturation. Under the action of pressure gradient and buoyancy, CO_2 migrated from the bottom of the reservoir to the top in a relatively short time and spread widely in the horizontal direction. Most of the CO_2 plume was still in the reservoir, and its diffusion range was about 250 m along the horizontal direction of the reservoir during the first ten years (Figure 6(a)). Only a small amount of CO_2 entered the upper reservoir, and the lateral migration distance was about 20 m. The maximum gas saturation in the whole caprock area was about 0.65 at the bottom of the upper caprock. After 50 years (Figure 6(b)), the CO_2 plume near the wellbore had passed through the top of the reservoir and entered mainly the upper caprock, about 90 m away from the bottom of the caprock, and the maximum CO_2 saturation reached 0.75. In the horizontal direction, CO_2 migrated far along with the reservoir-caprock interface, and its distribution range reached 450 m, which indicated that the bottom of the

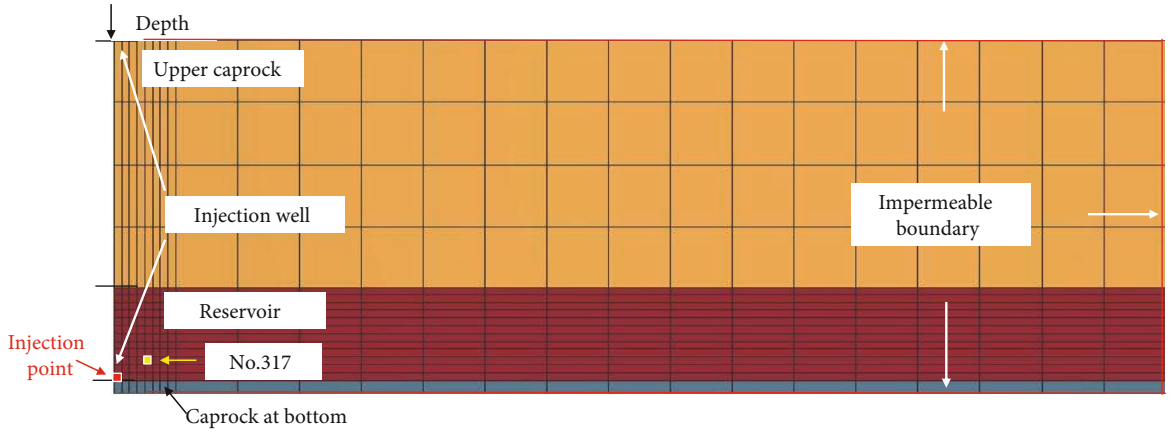

Figure 5: Schematic diagram of formation grid division.

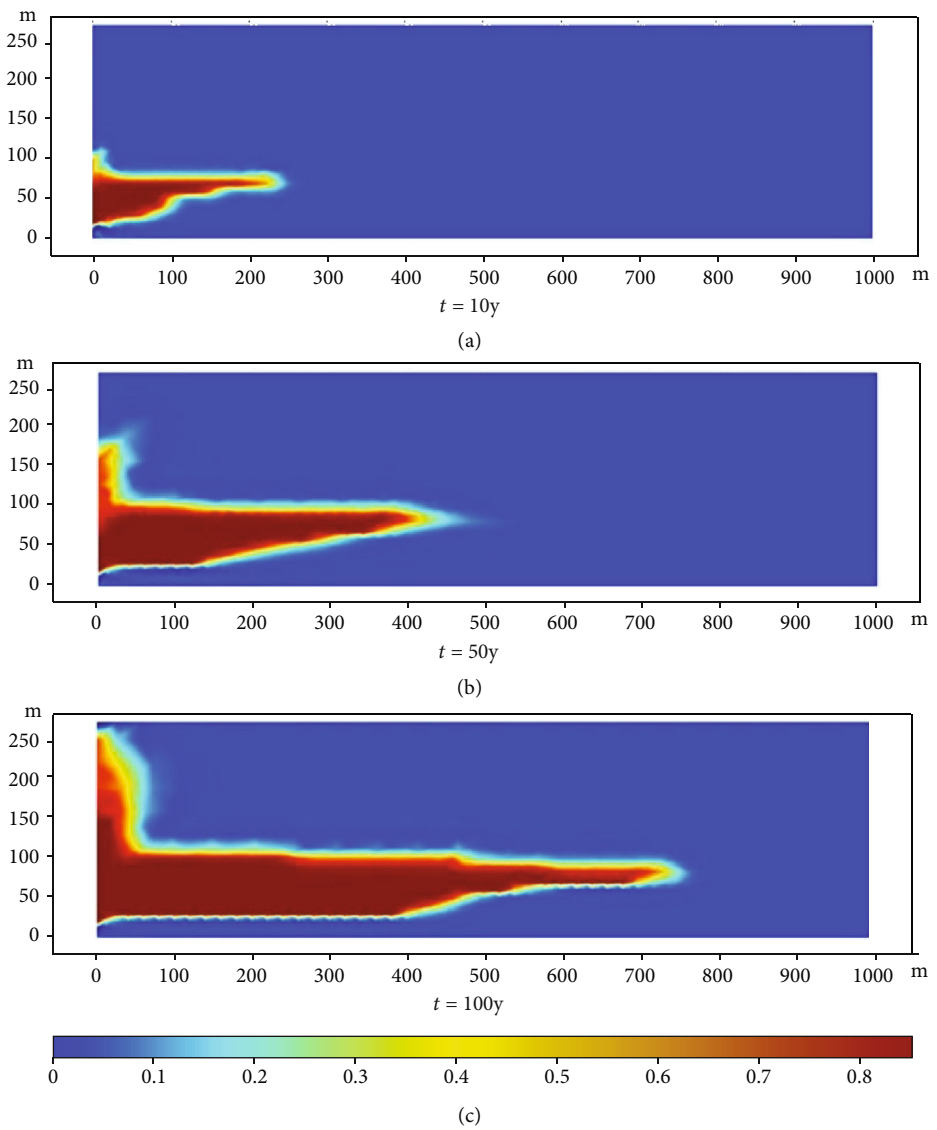

Figure 6: Migration of CO_2 in formation during 100 years storage.

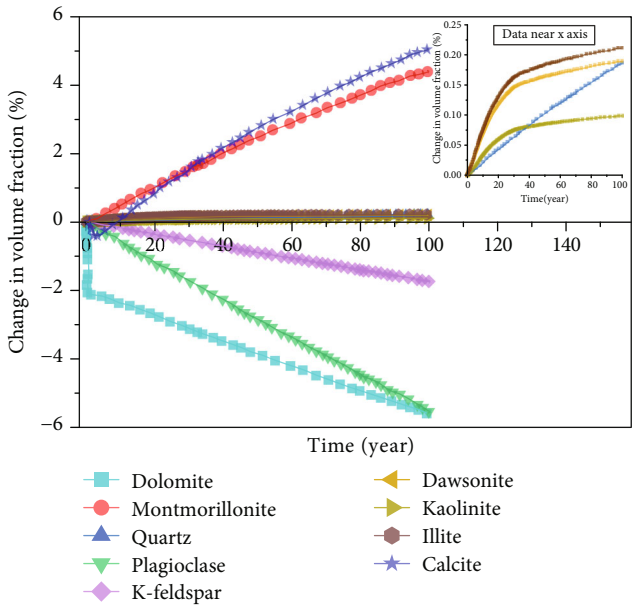

FIGURE 7: Volume fraction changes of minerals at monitoring grid.

caprock was subject to particular dissolution effect, and the risk of CO_2 leakage increase. The CO_2 had reached the top of the upper caprock 100 years later (Figure 6(c)), and the gas saturation is distributed within the range of 0.1~0.6. However, CO_2 saturation near the wellbore at the bottom of caprock reached 0.9, which had formed the CO_2 leakage channel. Moreover, the CO_2 concentration at reservoir-caprock interface had been large and distributed in a wide range, which proved that the bottom of the upper caprock had been seriously eroded, and the microscopic sealing ability had been greatly reduced. Especially, CO_2 near the injection well had reached the top of the caprock and there is a considerable risk of leakage.

3.2.2. Mineral Content, Porosity, and Permeability. No.317 grid was used as the monitoring grid, which was located at the bottom of the upper caprock near the injection point. The curves of mineral content, porosity, and permeability at this point are shown in Figures 7 and 8.

Under the acidic environment provided by CO_2, feldspar minerals mainly undergo dissolution reaction, accompanied by the precipitation of clay minerals. These minerals provided ions Ca^{2+}, Na^{+}, Mg^{2+}, and Fe^{2+} for the formation solution and then promoted the precipitation of kaolinite and quartz. At the early stage of the reaction, the content of dolomite tended to decrease from fast to slow, and the volume fraction of calcite decreased at the early stage of the reaction, and then increased. The reason may be that dolomite was a preferential dissolution. Although it provided Ca^{2+} for calcite precipitation, the dissolution rate of calcite was still higher than that of calcite precipitation. Therefore, the concentration of Ca^{2+} in formation solution remained stable, which was generally reflected as a dissolution phenomenon. As the reaction time went on, the dolomite continued to dissolve, leading to the increasing concentration of Ca^{2+} in the solution, inhibiting the dissolution of calcite, and leading to the reverse movement of calcite equilibrium reaction to generate precipitation. Although the change degree of mineral volume fraction varied in about 100 years, the amount of mineral dissolution was always more significant than that of precipitation.

The porosity and permeability had a similar increasing tendency; on the one hand, CO_2 increased the pore pressure and made the pores of caprock expand; on the other hand, the increase of porosity and permeability was caused by the particle volume reduction during the dissolution and precipitation of different minerals. According to the chemical kinetic reaction process, the dissolution amount of the primary mineral was greater than the precipitation amount of the secondary mineral, which increased the pore volume, porosity, and permeability of caprock, and gradually tended to be stable with the time of storage. However, the influence of CO_2 on the rock's physical properties will be finally reflected in the changes of rock microstructure such as pore radius, which further affects the breakthrough pressure of caprock.

3.2.3. Breakthrough Pressure. After CO_2 fluid filled the formation and chemical reaction occurs, the breakthrough pressure of formation decreased on the whole, and the distribution of breakthrough pressure at different positions was consistent with the expansion of CO_2 fluid. Equation (12) is used to calculate the distribution of the change value of breakthrough pressure caused by chemical reactions in the formation, as shown in Figure 9. After the simulation, due to the dominant role of dissolution in the whole reaction process, as the porosity and permeability increase, the rock breakthrough pressure at different positions decreases to various degrees. The rock breakthrough pressure corresponding to the location of the maximum CO_2 saturation decreased from 9.811 MPa to 6.20 MPa.

In the simulation process, CO_2 was not fully filled in the whole caprock layer, if the entire caprock is taken as the research object, the calculated average breakthrough pressure change value will be far less than the actual situation, so the caprock within 50 m of the horizontal distance from the injection point is taken as the research area, and the average breakthrough pressure of the caprock in this area is converted into the equivalent gas column sealing height by Equation (13) and the result is shown in Figure 10.

According to the evaluation index (Table 3), the microscopic sealing capacity of caprock downgraded from I to II. With the increase of storage time, the microscopic sealing ability will continue to reduce and cause irreversible damage.

To maintain the high microscopic sealing property of the caprock under the long-term CO_2 storage condition, the caprock with enough initial breakthrough pressure can be selected reasonably in the initial site selection according to the simulation results and index of gas sealing evaluation criteria. Because most of the caprocks contain natural cracks, microfissures, and fault systems, their physical sealing ability will be greatly reduced. Therefore, the actual microscopic

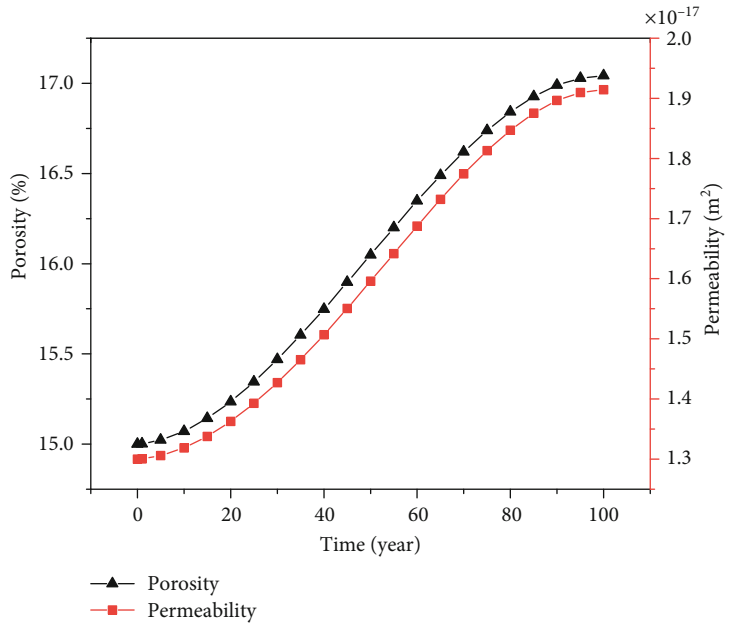

Figure 8: Changes of porosity and permeability at monitoring grid.

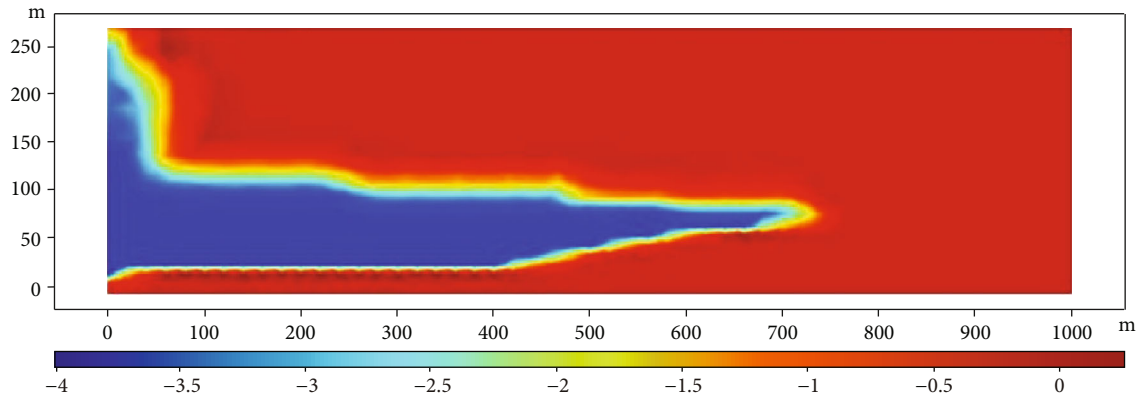

Figure 9: Changes of breakthrough pressure during 100 years storage.

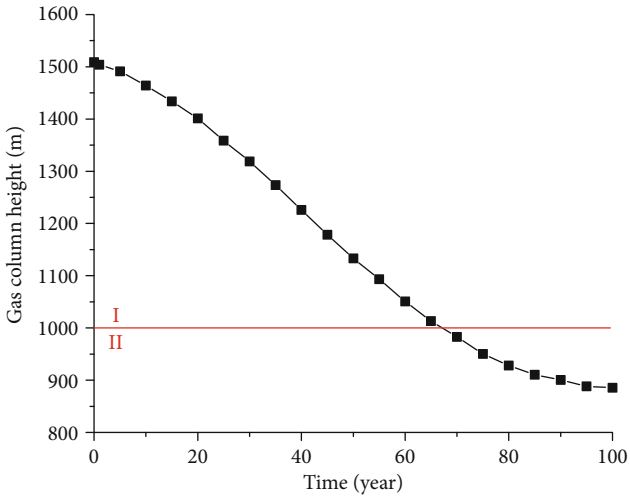

Figure 10: Changes of average caprock microsealing capacity.

sealing ability of caprocks will be generally lower than the theoretical value.

4. Conclusions

In this paper, a microscopic sealing evaluation method of caprock under CO_2 sequestration is established and the following insights are obtained:

(1) The essential change of the caprock microscopic sealing ability caused by CO_2 fluid is the change of microstructure, such as the rock pore radius. The breakthrough pressure of caprock after chemical reaction can be used as a dynamic evaluation index to predict the microscopic sealing property of the caprock under the action of chemical reaction accurately. It also provides an efficient and practical quantitative evaluation method for the initial site selection and safety storage evaluation in the later stage

Table 3: Classification standard of caprock microsealing capacity [25].

Level	I	II	III	IV
Height of closed gas column (m)	>1000	500~1000	200~500	<200

(2) The microscopic sealing property of the caprock after CO_2 storage is mainly related to the initial mineral composition of the rocks. The dissolution or precipitation amount of the caprocks composed of different minerals in the chemical reaction process is the crucial factor that determines the improvement or decrease of the microscopic sealing property

(3) The evaluation method in this paper was used to evaluate the effect of microsealing of mudstone caprock after CO_2 storage. The results show that the breakthrough pressure of the caprock decreases gradually with the increase of storage time, and the variation trend is roughly the same as that of porosity and permeability, indicating that the evaluation method can describe the dynamic microsealing capacity of caprock successfully

(4) Most of the formation rocks contain natural fractures and microfracture systems, and their microscopic sealing ability will be greatly reduced. Therefore, the macroscopic geological characteristics of the actual formation should be fully considered when evaluating the microscopic sealing ability of the caprocks

Data Availability

The data used to support the findings of this study are available from the corresponding author upon request.

Conflicts of Interest

The authors declare that they have no conflicts of interest.

Authors' Contributions

Xu Han is the first author.

Acknowledgments

This work is sponsored by the National Natural Science Foundation, China (No.51774094), China Postdoctoral Science Foundation (2018M641802), and the China Petroleum Science Technology Innovation Fund (2017D-5007-0310). This work is also supported by the "Thirteenth Five-Year Plan" National Science and Technology Major Project (No.2016ZX05016002) and Special Postdoctoral Funding in Heilongjiang Province, China (Postdoctoral Youth Excellence Scheme LBH-TZ12).

References

[1] Y. Hu, M. Hao, G. Chen, R. Sun, and S. Li, "Technologies and practice of CO_2 flooding and sequestration in China," *Petroleum Exploration and Development*, vol. 46, no. 4, pp. 753–766, 2019.

[2] I. C. Bourg, L. E. Beckingham, and D. J. Depaolo, "The nanoscale basis of CO_2 trapping for geologic storage," *Environmental Science & Technology*, vol. 49, no. 17, pp. 10265–10284, 2015.

[3] A. González-Nicolás, D. Baù, and B. M. Cody, "Application of binary permeability fields for the study of CO_2 leakage from geological carbon storage in saline aquifers of the Michigan Basin," *Mathematical Geosciences*, vol. 50, no. 5, article 9706, pp. 525–547, 2018.

[4] B. Orlic, "Geomechanical effects of CO_2 storage in depleted gas reservoirs in the Netherlands: inferences from feasibility studies and comparison with aquifer storage," *Journal of Rock Mechanics and Geotechnical Engineering*, vol. 8, no. 6, pp. 846–859, 2016.

[5] N. Castelletto, G. Gambolati, and P. Teatini, "Geological CO2sequestration in multi-compartment reservoirs: geomechanical challenges," *Journal of Geophysical Research: Solid Earth*, vol. 118, no. 5, pp. 2417–2428, 2013.

[6] D. G. Hatzignatiou, F. Riis, R. Berenblyum, V. Hladik, R. Lojka, and J. Francu, "Screening and evaluation of a saline aquifer for CO_2 storage: Central Bohemian Basin, Czech Republic," *International Journal of Greenhouse Gas Control*, vol. 5, no. 6, pp. 1429–1442, 2011.

[7] F. Gherardi, T. Xu, and K. Pruess, "Numerical modeling of self-limiting and self-enhancing caprock alteration induced by CO_2 storage in a depleted gas reservoir," *Chemical Geology*, vol. 244, no. 1-2, pp. 103–129, 2007.

[8] Y. Li, H. L. Tian, Z. Zhuo, and Y. Sun, "The potential effect of CO_2-water-rock reaction on the caprock formation (*Mudstone*) case study," *Advanced Materials Research*, vol. 518-523, pp. 140–143, 2012.

[9] W. Kong, B. Bai, X. Li, and N. Wei, "Sealing efficiency of combined caprock for CO_2 storage in saline aquifer," *Chinese Journal of Rock Mechanics and Engineering*, vol. 34, pp. 2671–2678, 2015.

[10] T. Fristad, A. Groth, G. Yielding, and B. Freeman, "Quantitative fault seal prediction: a case study from Oseberg Syd," *Norwegian Petroleum Society Special Publications*, vol. 7, no. 97, pp. 107–124, 1997.

[11] B. Soleimani, M. Hassani-Giv, and I. A. Fard, "Formation pore pressure variation of the Neocomian sedimentary succession (the Fahliyan Formation) in the Abadan Plain Basin, SW of Iran," *Geofluids*, vol. 2017, 13 pages, 2017.

[12] M. Claprood, E. Gloaguen, M. Sauvageau, B. Giroux, and M. Malo, "Adapted sequential Gaussian simulations with Bayesian approach to evaluate the CO2storage potential in low porosity environment," *Greenhouse Gases Science and Technology*, vol. 4, no. 6, pp. 761–776, 2015.

[13] C. Chalbaud, M. Robin, J. M. Lombard, F. Martin, P. Egermann, and H. Bertin, "Interfacial tension measurements and wettability evaluation for geological CO_2 storage," *Advances in Water Resources*, vol. 32, no. 1, pp. 98–109, 2009.

[14] A. T. Mccay, R. J. Lunn, and Z. K. Shipton, "Connected subseismic features compromise cap rock integrity: the influence of faults and permeable sandstone lenses," *Journal of Human Resources*, vol. 20, no. 3, pp. 421–436, 2011.

[15] W. A. Ambrose, S. Lakshminarasimhan, M. H. Holtz, V. Núñez-López, S. D. Hovorka, and I. Duncan, "Geologic factors controlling CO_2 storage capacity and permanence: case studies based on experience with heterogeneity in oil and gas reservoirs applied to CO_2 storage," *Environmental Geology*, vol. 54, no. 8, pp. 1619–1633, 2008.

[16] M. Ashraf, S. Oladyshkin, and W. Nowak, "Geological storage of CO_2: application, feasibility and efficiency of global sensitivity analysis and risk assessment using the arbitrary polynomial chaos," *International Journal of Greenhouse Gas Control*, vol. 19, pp. 704–719, 2013.

[17] J. Schneider, P. B. Flemings, R. J. Day-Stirrat, and J. T. Germaine, "Insights into pore-scale controls on mudstone permeability through resedimentation experiments," *Geology*, vol. 39, no. 11, pp. 1011–1014, 2011.

[18] H. Ott, K. de Kloe, M. van Bakel et al., "Core-flood experiment for transport of reactive fluids in rocks," *Review of Scientific Instruments*, vol. 83, no. 8, article 084501, 2012.

[19] B. R. Ellis, J. P. Fitts, G. S. Bromhal, D. McIntyre, R. Tappero, and C. A. Peters, "Dissolution-driven permeability reduction of a fractured carbonate caprock," *Environmental Engineering Science*, vol. 30, no. 4, pp. 187–193, 2013.

[20] M. Angeli, M. Soldal, E. Skurtveit, and E. Aker, "Experimental percolation of supercritical CO_2 through a caprock," *Energy Procedia*, vol. 1, no. 1, pp. 3351–3358, 2009.

[21] M. Cunfei, D. Chunmei, L. Chengyan et al., "Calculation method and application of cap rock's effective thickness," *Journal of China University of Petroleum*, vol. 42, no. 1, p. 21, 2018.

[22] H. Yamabe, T. Tsuji, Y. Liang, and T. Matsuoka, "Lattice Boltzmann simulations of supercritical CO2-water drainage displacement in porous media: CO_2 saturation and displacement mechanism," *Environmental Science & Technology*, vol. 49, no. 1, pp. 537–543, 2015.

[23] F. Guang and Q. FXM, "Research of capillary seal ability and its formation period of mudstone caprock with acoustic transit time," *Geophysical Prospecting for Petroleum*, vol. 2, pp. 261–264, 2003.

[24] Z. Cheng, *Breakthrough Pressure and Permeability Characteristics of Unsaturated Shales from Eastern Qaidam Basin, China*, China University of Geosciences, Beijing, 2018.

[25] X. Zhou, X. Lü, H. Quan et al., "Influence factors and an evaluation method about breakthrough pressure of carbonate rocks: an experimental study on the Ordovician of carbonate rock from the Kalpin area, Tarim Basin, China," *Marine and Petroleum Geology*, vol. 104, pp. 313–330, 2019.

[26] C. M. Bethke, "Geochemical reaction modeling: concepts and applications," *Oxford University Press*, vol. 53, no. 2, pp. 205–214, 1996.

[27] Y. K. Kharaka, *Water-Rock Interaction*, A.A. Balkema, 1992.

[28] J. A. Businger and A. C. Delany, "Chemical sensor resolution required for measuring surface fluxes by three common micrometeorological techniques," *Journal of Atmospheric Chemistry*, vol. 10, no. 4, pp. 399–410, 1990.

[29] J. Bear, *Dynamics of Fluids in Porous Media*, Dover Publications, Inc., New York, NY, USA, 1972.

[30] L. Chuanliang, "Effect of poro-throat ratio on reservoir permeablity," *Petroleum Geology and Recovery Efficiency*, vol. 14, no. 5, pp. 78-79, 2007.

[31] B. Zheng and L. Juhua, "A new fractal permeability model for porous media based on Kozeny-Carman equation," *Natural Gas Geoscience*, vol. 26, no. 1, pp. 193–198, 2015.

[32] Z. Dewen, "Establishment of natural gas caprock capillarity evaluation criteria," *Natural Gas Geoscience*, vol. 5, no. 3, pp. 29–33, 1994.

[33] A. Tanaka, Y. Sakamoto, and T. Komai, "Development of risk assessment tool for CO_2 geological storage," *Energy Procedia*, vol. 4, pp. 4178–4184, 2011.

[34] L. Zhang, R. M. Dilmore, and G. S. Bromhal, "Effect of outer boundary condition, reservoir size, and CO_2 effective permeability on pressure and CO_2 saturation predictions under carbon sequestration conditions," *Greenhouse Gases: Science and Technology*, vol. 6, no. 4, pp. 546–560, 2016.

[35] A. C. Lasaga, *Kinetic Theory in the Earth Sciences*, Princeton University Press, 2014.

[36] D. C. Mangold and C. F. Tsang, "A summary of subsurface hydrological and hydrochemical models," *Reviews of Geophysics*, vol. 29, no. 1, p. 51, 1991.

[37] E. Busenberg and L. N. Plummer, "The kinetics of dissolution of dolomite in CO_2-H_2O systems at 1.5 to 65°C and 0 to 1 atm PCO_2," *American Journal of Science*, vol. 282, no. 1, pp. 45–78, 2011.